The 4th European sCO_2 Conference for Energy Systems
March 23-24, 2021, Online Conference

2021-sCO2.eu-131

STUDY OF THE INFLUENCE OF ADDITIVES TO CO_2 ON THE PERFORMANCE PARAMETERS OF A SCO2-CYCLE

Sebastian Rath*
TU Dresden
Dresden, Germany
Email: sebastian.rath@tu-dresden.de

Erik Mickoleit
TU Dresden
Dresden, Germany

Uwe Gampe
TU Dresden
Dresden, Germany

Cornelia Breitkopf
TU Dresden
Dresden, Germany

Andreas Jäger
TU Dresden
Dresden, Germany

ABSTRACT
Compared to existing technologies, thermodynamic cycles based on supercritical carbon dioxide (sCO_2) are leading to higher efficiencies and a more compact design of the components. However, it is possible to improve the performance of sCO_2-based power cycles by using mixtures of CO_2 with suitable additives, as also discussed in the literature for some applications such as concentrated solar power plants or the usage of geothermal heat.
The large variety of possible fluid combinations makes an experimental investigation of all conceivable additives considerably difficult. Therefore, a more viable alternative is to set up a model for the power cycle and conduct a screening in order to identify promising candidates for working fluid mixtures. In a next step these could subsequently be experimentally verified. In order to carry out a screening, a preferably accurate and likewise predictive mixture model is needed.
This work investigates the potential to optimize the characteristics of sCO_2 power cycles by selectively adding different substances in varying amounts to CO_2. For the theoretical screening, the reference equation of state for CO_2 was applied in combination with a multi-fluid mixture model. In the literature studies were mainly limited to mixtures for which adjusted mixture models are available. In contrast, in this work the use of a predictive mixture model allows a screening of additional fluids for which multi-parameter equations of state are available (e.g. alkanes, alkenes, alcohols, and hydrofluoro-carbons). The predictive model, which was recently developed at our institute, allows the use of the excess Gibbs energy model COSMO-SAC in combination with the multi-fluid mixture model. Applied to an exemplary thermodynamic cycle, changes in efficiency compared to the use of pure CO_2 have been evaluated. Several promising mixture candidates have been identified. Additionally, shifts of the critical point have been investigated and are discussed.

INTRODUCTION
The usage of supercritical CO_2 (sCO_2) as a working fluid in power cycles, such as concentrated solar power plants, waste-heat recovery, or nuclear plants, is a current topic in science and industry [1–4]. SCO_2 offers some distinct advantages when compared to other working fluids. For example, due its liquid-like density in the supercritical state, components of the power cycle become significantly smaller than components of a comparable steam cycle. Furthermore, due to the relatively low critical temperature of CO_2 ($\vartheta_c \approx 31\,°C$), sCO_2 can also be utilized as a working fluid when the heat source has a relatively low temperature, as for example in geothermal applications [1].
However due to the strong variation of fluid properties near the critical point, even small changes in the conditions at the inlet can cause large deviations in efficiency. Consequently, appropriate solutions must be found to ensure stable process parameters even under changing environmental conditions without cutting back the efficiency too much. In this context one option could be the use of mixtures that have a less dynamic variation of the fluid properties in the considered range.

While the advantages of pure CO_2-cycles have already been studied quite extensively in the literature [5–7], the application of mixtures with CO_2 has not been studied to the same extend yet. Baik and Lee [8] investigated a simple Brayton cycle and investigated the influence of six additives (SF_6, R-123, R-134a, R-22, R-32, and toluene) to CO_2 on several performance parameters of the cycle. They used equations of state implemented in the thermophysical property software NIST REFPROP (2010) as well as an in-house software in order to calculate the properties of the mixtures. Baik and Lee found R-

* corresponding author(s)

DOI: 10.17185/duepublico/73965

32 to be the most promising additive for the simple Brayton cycle and conducted experiments for the binary mixture of CO_2+R-32 in order to confirm their results. They conclude that R-32 and toluene are promising candidates that could reduce the decrease of efficiency in summer due to higher cooling temperatures. Binotti et al. [9,10] used the Peng-Robinson equation of state implemented in AspenPlus v9.0 in order to investigate the application of the mixtures CO_2 + $TiCl_4$ and CO_2 + N_2O_4 as working fluids in solar power plants. For some of the investigated mixture compositions and boundary conditions of the process, Binotti et al. [9,10] found that the efficiency of the process can be increased when using mixtures compared to the efficiency when using pure CO_2 as working fluid. Manzolini et al. [11] investigated the effect of using mixtures of CO_2 + $TiCl_4$ and CO_2 + N_2O_4 instead of pure CO_2 on the levelized cost of electricity for solar power plants. They also used the Peng-Robinson equation of state in order to calculate the properties of the mixtures and found that, according to their calculations, the mixture of CO_2 with either N_2O_4 or $TiCl_4$ are promising candidates to reach lower levelized costs of electricity as compared to solar power plants with pure CO_2 as working fluid. However, they also note that relatively simple equations of state (i.e. the Peng-Robinson equation of state) have been used in their model in order to calculate the results and therefore, the results need further validation.

Recently, our group has developed a predictive combination of the multi-fluid mixture model with excess Gibbs energy models (g^{E}-models) [12,13]. In this model, the best equations of state available for the pure substances, for example the reference equation of state for CO_2 by Span and Wagner [14], can be used together with best available predictive models, such as the g^{E}-models UNIFAC [15] or COSMO-SAC [16–18]. It has already been demonstrated that this model yields good results when used for a screening in refrigeration cycles [19,20]. In this work, the predictive mixture model is applied to a power cycle for the first time. Two different configurations of the power cycle were studied and all substances for which accurate multi-parameter equations of state are available have been considered as additives to CO_2.

MIXTURE MODELS

In this work, multi-fluid mixture models have been used to calculate the thermophysical properties of the various CO_2 mixtures, which have been considered as alternative working fluids for two different power cycle configurations as discussed in the subsequent section. The multi-fluid mixture model, as proposed by Lemmon and Tillner-Roth [21] and developed further by Kunz et al. [22,23], Gernert and Span [24], and Herrig [25] reads

$$\alpha(\tau,\delta,\vec{x}) = \sum_{i=1}^{N} x_i[\alpha_{\mathrm{o}i}^{0}(\rho,T) + \ln(x_i) + \alpha_{\mathrm{o}i}^{\mathrm{r}}(\delta,\tau)] + \sum_{i=1}^{N-1}\sum_{j=i+1}^{N} x_i x_j F_{ij}\alpha_{ij}^{\mathrm{r}}(\tau,\delta)\,. \quad (1)$$

where α denotes the dimensionless Helmholtz energy, $\vec{x}$ is the vector of mole fractions in the mixture with x_i denoting the mole fraction of component i, N is the number of components in the mixture, T is the temperature and ρ is the density. $\alpha_{\mathrm{o}i}^{0}$ denotes the ideal part and $\alpha_{\mathrm{o}i}^{\mathrm{r}}$ the residual part of the dimensionless Helmholtz energy of component i in the mixture. α_{ij}^{r} is the binary specific departure function for components i and j in the mixture and F_{ij} are parameters of the binary specific departure functions. The inverse reduced temperature τ is defined as

$$\tau = T_{\mathrm{r}}/T \quad (2)$$

and the reduced density can be calculated according to the relation

$$\delta = \rho/\rho_{\mathrm{r}} \quad (3)$$

The reducing temperature T_{r} and the reducing density ρ_{r} are calculated with the functional forms proposed by Klimeck [26] and Kunz et al. [22,23], which read

$$T_{\mathrm{r}} = \sum_{i=1}^{N}\sum_{j=1}^{N} x_i x_j \beta_{T,ij}\gamma_{,Tij}\frac{x_i + x_j}{\beta_{T,ij}^{2}x_i + x_j}\left(T_{\mathrm{c},i}\cdot T_{\mathrm{c},j}\right)^{0.5} \quad (4)$$

and

$$\frac{1}{\rho_{\mathrm{r}}} = \sum_{i=1}^{N}\sum_{j=1}^{N} x_i x_j \beta_{v,ij}\gamma_{,vij}\frac{x_i + x_j}{\beta_{v,ij}^{2}x_i + x_j}\frac{1}{8}\left(\rho_{\mathrm{c},i}^{-\frac{1}{3}} + \rho_{\mathrm{c},j}^{-\frac{1}{3}}\right)^{3}. \quad (5)$$

$\beta_{T,ij}$, $\gamma_{,Tij}$, $\beta_{v,ij}$, and $\gamma_{,vij}$ are adjustable parameters for each binary pair of components i and j in the mixture, T_{c} are the critical temperatures and ρ_{c} the critical densities of the components in the mixture. One of the main advantages of this mixture model is its flexibility. The residual part of the dimensionless Helmholtz energy $\alpha_{\mathrm{o}i}^{\mathrm{r}}$ required in Equation (1) can be calculated from highly accurate multiparameter equations of state, such as the reference equation of state for CO_2 by Span and Wagner [14]. However, if no multiparameter equation of state is available for a component i in the mixture, any other equation of state could be translated to the dimensionless Helmholtz energy. As an example, Bell and Jäger [27] provide Helmholtz energy translations of common cubic equations of state, i.e., the Soave-Redlich Kwong equation of state (SRK) [28,29] and the Peng-Robinson equation of state (PR) [30].

In this work, only substances for which multiparameter equations of state are available, have been considered as additives to CO_2 in order to increase the efficiency of the power cycles discussed in the following section. The considered substances and the multiparameter equations of state used [31–81] to calculate thermophysical properties for these substances are listed in Table A in Annex A: Note that for some of the considered substances unpublished equations of state are available in NIST REFPROP 10.0 [31], which have been used in this work.

For some mixtures of CO_2 with other substances multi-fluid mixture models with adjusted parameters are available, see, e.g., Gernert and Span [24], Kunz et al. [23], or Herrig [25]. However, for many mixtures considered in this screening no multi-fluid mixture model with adjusted parameters are available in the literature. Therefore, these mixtures need to be modeled

predictively with the multi-fluid mixture model. The simplest possibility of using the multi-fluid mixture model predictively is omitting the departure function in Equation (1), i.e., $\alpha_{ij}^{\mathrm{r}} = 0$. For the reducing temperature T_{r} and the reducing density ρ_{r} either linear mixing rules or Lorentz-Berthelot combining rules can be used, see [22]. Linear mixing rules yield

$$T_{\mathrm{r}} = \sum_{i=1}^{N} x_i T_{\mathrm{c},i} \tag{6}$$

and

$$\frac{1}{\rho_{\mathrm{r}}} = v_{\mathrm{r}} = \sum_{i=1}^{N} x_i v_{\mathrm{c},i} = \sum_{i=1}^{N} x_i \frac{1}{\rho_{\mathrm{c},i}} \tag{7}$$

and Lorentz-Berthelot combining rules are used by setting

$$\beta_{T,ij} = 1,\ \gamma_{T ij} = 1,\ \beta_{v,ij} = 1, \text{ and } \gamma_{,vij} = 1. \tag{8}$$

However, linear mixing rules and Lorentz-Berthelot combining rules often do not yield good predictive results, as for example demonstrated by Jäger et al. [12,13,82]. Therefore, a recently developed combination of multi-fluid mixture models with g^{E}-models by Jäger et al. [12,13] has been applied to predictively calculate mixture properties. The multi-fluid mixture model in combination with a theoretically-based departure function that depends on a g^{E}-model reads

$$\begin{aligned}\alpha(\tau,\delta,\vec{x}) = &\sum_{i=1}^{N} x_i[\alpha_{\mathrm{o}i}^{0}(\rho,T) + \ln(x_i) + \alpha_{\mathrm{o}i}^{\mathrm{r}}(\delta,\tau)] \\ &+ \frac{\ln(1+b\rho)}{\ln(1+b\rho_{\mathrm{ref}})}\left[\frac{g_{\mathrm{GE}}^{\mathrm{E,r}}}{RT}\right. \\ &\left. - \sum_{i=1}^{N} x_i\left[\alpha_{\mathrm{o}i}^{\mathrm{r}}(\delta_{\mathrm{ref}},\tau) - \alpha_{\mathrm{o}i}^{\mathrm{r}}(\delta_{i,\mathrm{ref}},\tau_i)\right]\right].\end{aligned} \tag{9}$$

In Equation (8), b denotes the co-volume of the mixture, see [13], according to

$$b = \sum_{i=1}^{N} x_i b_i \tag{10}$$

with b_i being modified co-volumes of the components i in the mixture (see [13])

$$b_i = \frac{v_{\mathrm{s},i}^{\mathrm{L}}}{u} \tag{11}$$

with $u = 1.17$ denoting the inverse packing fraction and $v_{\mathrm{s},i}^{\mathrm{L}}$ is the molar volume of the saturated liquid of component i at the reference pressure p_0 = 101325 Pa. The density ρ_{ref} at p_0 is given by the linear mixing rule

$$\frac{1}{\rho_{\mathrm{ref}}} = \sum_{i=1}^{N} x_i v_{\mathrm{s},i}^{\mathrm{L}}. \tag{12}$$

In Equation (8), $g_{\mathrm{GE}}^{\mathrm{E,r}}$ denotes the residual part of the excess Gibbs energy, which in this work has been calculated with the COSMO-SAC model by Hsieh et al. [18].

The model COSMO-SAC was published by Lin and Sandler [16,17] and is a modification of the conductor-like screening model for real solvents (COSMO-RS) developed by Klamt et al. [83–85]. The COSMO-SAC model used in this work is the model proposed by Hsieh et al. [18], which is an improvement of the original COSMO-SAC model by Lin and Sandler [16]. The residual excess Gibbs energy $g_{\mathrm{GE}}^{\mathrm{E,r}}$ can be obtained by the relation

$$g_{\mathrm{GE}}^{\mathrm{E,r}} = RT \sum_{i=1}^{N} x_i \ln(\gamma_{i,\mathrm{S}}^{\mathrm{r}}), \tag{13}$$

where $\gamma_{i,\mathrm{S}}^{\mathrm{r}}$ is the residual activity coefficient of component i in a liquid system S. According to the COSMO-SAC model suggested by Hsieh et al. [18], $\gamma_{i,\mathrm{S}}^{\mathrm{r}}$ can be calculated by the relation

$$\begin{aligned}\ln\left(\gamma_{i,\mathrm{S}}^{\mathrm{r}}\right) = n_i \sum_{t}^{\mathrm{nhb,OT,OH}} \sum_{\sigma_m} p_i^t(\sigma_m^t)\left[\ln\left(\Gamma_{\mathrm{S}}^t(\sigma_m^t)\right)\right. \\ \left. - \ln\left(\Gamma_i^t(\sigma_m^t)\right)\right].\end{aligned} \tag{14}$$

The input required to evaluate Equation (14) are COSMO-calculations for each component in the mixture of interest, see Klamt and Schüürmann [86]. The model assumes that the molecule is placed in a perfect conductor and subsequently screening charges σ are calculated on a molecule-shaped cavity. The obtained screening charges are averaged on a standard surface in order to obtain the screening charges σ_m of the standard segments m, see [18,87]. In Equation (14), n_i denotes the number of standard surface segments of molecule i. $p_i(\sigma_m)$ is the σ-profile of molecule i, which describes the probability of finding a segment with screening charge density σ_m on the surface of molecule i. It is defined by

$$p_i(\sigma_m) = \frac{A_i(\sigma_m)}{A_i}, \tag{15}$$

with A_i being the surface area of molecule i according to the COSMO-calculation and $A_i(\sigma_m)$ denoting the surface area of molecule i with a surface charge density σ_m. In the COSMO-SAC model of Hsieh et al. [18], the σ-profile is split into three contributions, a non-hydrogen-bonding part $p_i^{\mathrm{nhb}}\left(\sigma_m^{\mathrm{nhb}}\right)$ and two hydrogen-bonding profiles considering hydrogen-bonding of hydroxyl groups $p_i^{\mathrm{OH}}(\sigma_m^{\mathrm{OH}})$ and hydrogen-bonding of other atoms $p_i^{\mathrm{OT}}(\sigma_m^{\mathrm{OT}})$. It is

$$p_i(\sigma) = p_i^{\mathrm{nhb}}(\sigma) + p_i^{\mathrm{OH}}(\sigma) + p_i^{\mathrm{OT}}(\sigma)\,. \tag{16}$$

More detailed information on how the sigma-profiles are generated from the COSMO-calculations can be taken from [18,87]. For illustration, the σ-profile and the screening charge densities for CO_2 are displayed in Figure 1.

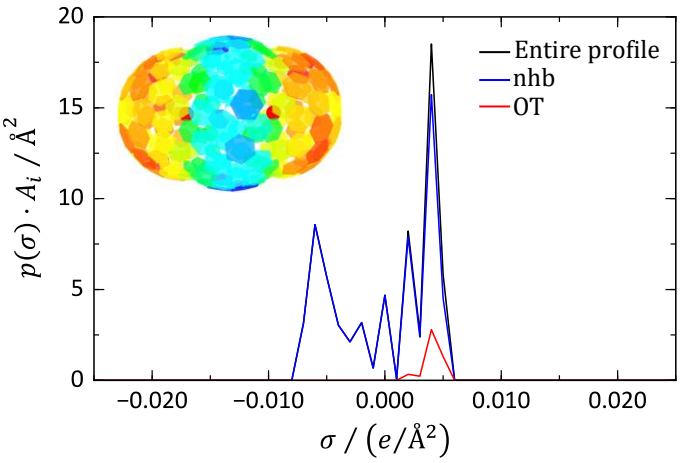

Figure 1: Screening charge densities for CO_2 (colored hexagons) from COSMO-calculations taken from the database by Bell et al. [87] and σ-profile multiplied by the surface area A_i ("Entire profile", solid black line) split into the non-hydrogen-bonding ("nhb", solid blue line) and hydrogen-bonding ("OT", solid red line) part.

The segment activity coefficients of the segments m belonging to profile t in the mixture $\Gamma_S^t(\sigma_m^t)$ can be calculated from the system of equations

$$\ln\left(\Gamma_S^t(\sigma_m^t)\right) = -\ln\left\{\sum_s^{\text{nhb,OH,OT}} \sum_{\sigma_n} p_S^s(\sigma_n^s)\Gamma_S^s(\sigma_n^s) \cdot \exp\left[-\frac{\Delta W(\sigma_m^t, \sigma_n^s)}{RT}\right]\right\}. \quad (17)$$

The σ-profiles $p_S^s(\sigma_n^s)$ of the mixture can be calculated according to

$$p_S^s(\sigma_n^s) = \frac{\sum_{i=1}^N x_i A_i p_i(\sigma_n^s)}{\sum_{i=1}^N x_i A_i}. \quad (18)$$

The exchange energy $\Delta W(\sigma_m^t, \sigma_n^s)$ of two surface segments m and n can obtained from the electrostatic and hydrogen-bonding contribution

$$\Delta W(\sigma_m^t, \sigma_n^s) = \left(A_{\text{ES}} + \frac{B_{\text{ES}}}{T^2}\right)(\sigma_m^t + \sigma_n^s)^2 - c_{\text{hb}}(\sigma_m^t - \sigma_n^s)^2. \quad (19)$$

A_{ES}, B_{ES}, and c_{hb} are constants of the model, which are given by Hsieh et al. [18]. Finally, the segment activity coefficients of the segments m belonging to a profile t if only pure component i is present can be calculated by solving the system of equations

$$\ln\left(\Gamma_i^t(\sigma_m^t)\right) = -\ln\left\{\sum_s^{\text{nhb,OH,OT}} \sum_{\sigma_n} p_i^s(\sigma_n^s)\Gamma_i^s(\sigma_n^s) \cdot \exp\left[-\frac{\Delta W(\sigma_m^t, \sigma_n^s)}{RT}\right]\right\}. \quad (20)$$

All equations of state used in this work are available in the thermophysical property software TREND 4.0 [88]. The COSMO-files for all components studied in this work have been taken from the database provided by Bell et al. [87], which is an extension of the database of Mullins et al. [89]. The algorithms for phase equilibrium calculations with TREND are described in the works of Gernert et al. [90] and Jäger [91].

CYCLE MODELING

For comparison of the mixtures, two different sCO_2 cycle architectures have been chosen. As shown in Figure 2, the first layout consists of a simple cycle including only the essential main components. Starting at the compressor inlet in point 1, the fluid is compressed to the upper pressure level at point 2. Subsequently, heat is added in an isobaric heater until the upper temperature level is reached in point 3 corresponding to the turbine inlet. After expansion to point 4, excess heat is rejected in a cooler going back to the starting conditions. Figure 2 shows the second layout, in which a recuperator extends the simple cycle. In this way, a part of the heat at the turbine outlet (point 5) is transferred back to the compressed fluid (point 2) reducing the amount of heat to be added in the heater.

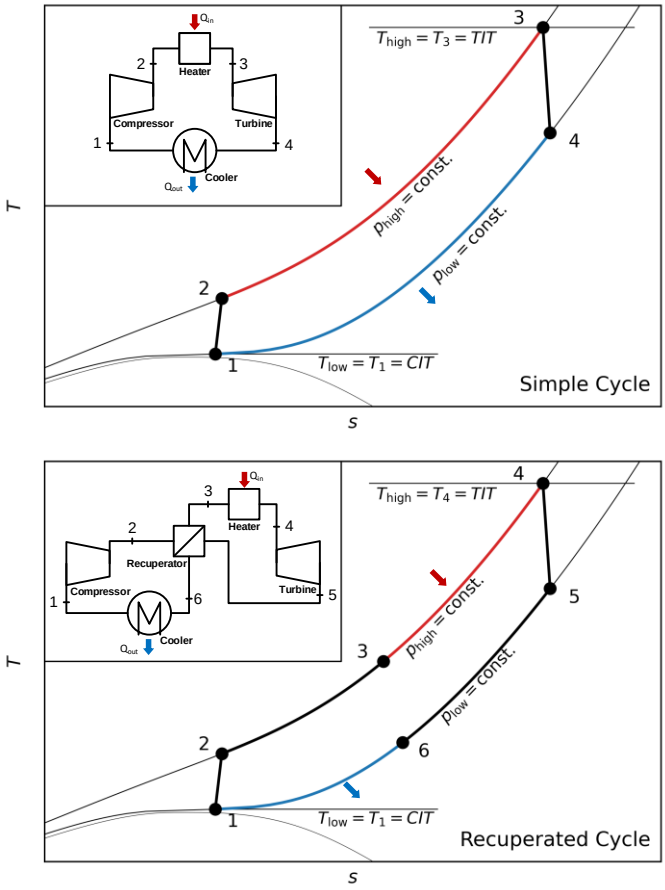

Figure 2: Block diagrams and T-s diagrams of the considered cycle architectures.

The recuperation in the second cycle was modeled by setting a minimum pinch point difference at the cold end of the recuperator, i.e., $T_6 = T_2 + \Delta T_R$, where ΔT_R denotes the temperature difference at the pinch point. In addition to that, a simplified check if the pinch point is violated anywhere along the recuperator has been done by a stepwise calculation of the heat transfer. Using the mixture models described before, calculations were done for both layouts based on preset values for pressure and temperature at the inlets of the compressor and the turbine. Beside all relevant fluid properties, such as enthalpy or density, the number and type of simultaneously present thermodynamic phases at each state point as well as the mixtures boiling temperature at both pressure levels were calculated. For comparison of the working fluids, the thermal efficiency was used which can be calculated by the relation

$$\eta_{th,SC} = 1 - \frac{h_4 - h_1}{h_3 - h_2} \quad (21)$$

for the simple cycle and

$$\eta_{th,RC} = 1 - \frac{h_6 - h_1}{h_4 - h_3} \quad (22)$$

for the recuperated cycle. The boundary conditions applied to the thermodynamic cycles are listed in Table 1.

Table 1: Boundary conditions applied to the process calculations.

Boundary condition	Symbol	Value
Minimum temperature	$\vartheta_{low} \equiv$ CIT	31 … 40 °C
Maximum temperature	$\vartheta_{high} \equiv$ TIT	500 °C
Lower pressure level	p_{low}	7.4 MPa
Upper pressure level	p_{high}	20 MPa
Compressor efficiency	η_C	0.8
Turbine efficiency	η_T	0.9
Min. pinch point difference recuperator	ΔT_R	10 K

Temperatures were oriented to an exemplary waste heat recovery application with possible air-recooling to ambient conditions. The lower temperature level has been varied within a range of 31 °C to 40 °C while the upper temperature has been fixed at 500 °C. The lower temperature corresponds to the temperature at the compressor inlet and the upper temperature is the temperature at the turbine inlet. Pressure levels were set to a near critical value of 7.4 MPa for the lower pressure level and 20 MPa for the upper pressure level. Losses were treated in terms of isentropic efficiencies for the compressor and the turbine. For the recuperator, a minimum pinch point difference of 10 K was applied. Pressure losses were completely neglected. In all cases, the operation of both process architectures of the cycle with pure CO_2 was used as a basis for comparison. With reference to the considered temperature range of $\vartheta_{low} = 31 \ldots 40$ °C at the compressor inlet, Figure 3 shows the changes (differences) in thermal efficiency compared to $\vartheta_{low} = 31$ °C representing the temperature closest to the critical point regarding the set boundary conditions. As can be seen in the graph, with the exception of a small peak just above 31 °C, the efficiency drops significantly with increasing inlet temperature. At 40 °C, a decrease of about 6% for the simple cycle and about 4% for the recuperated cycle can be noted. The aforementioned small increases are due to the pseudo-critical point at the chosen pressure of p_{low} =7.4 MPa, which is slightly higher than the critical pressure p_c =7.3773 MPa [92].

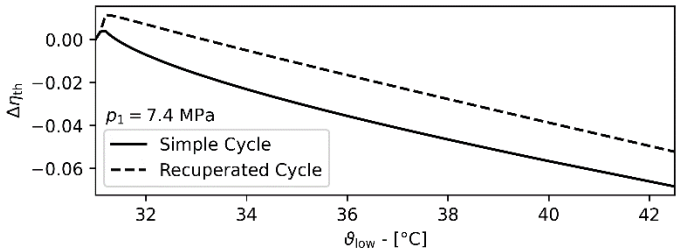

Figure 3: Difference of the thermal efficiencies calculated with varying ϑ_{low} and the thermal efficiency for $\vartheta_{low} = 31$ °C for the simple cycle and the recuperated cycle with pure CO_2. All other boundary conditions have been set according to the values listed in Table 1.

RESULTS AND DISCUSSION

To identify promising mixing partners for a more detailed examination, calculations were done for a total of 135 fluids and for a compressor inlet temperature of 40 °C, which corresponds to the most inefficient inlet conditions regarding the boundary conditions specified in this work, see Table 1, and the usage of pure CO_2, see Figure 3. Since multiphase flows might lead to problems, for example in the compressor or turbine, this study has been restricted to mixtures that do not decompose into several phases at the state points of the cycle. This means that all mixtures existing in more than one phase in any of the state points of the process have been excluded from this study. In addition to that, concerning the recuperated case, all combinations leading to pinch-point violations in the recuperator were also discarded. Figure 4 shows the results for the remaining 111 fluids in terms of the change in efficiency as a function of the mole fraction of the mixture. Starting with the groups of alkenes, alkynes, and alkanes it can be seen that for the simple cycle configuration almost all substances cause a reduction in efficiency with increasing mole fraction. However, a small improvement in the efficiency is obtained when adding up to 5% of propyne, see Figure 4a. A slightly positive trend can also be assumed for propadiene, although to a lesser extent. For both of these fluids, the mixtures decompose in two phases for the studied mole fractions higher than 5%. In contrast, an opposite pattern regarding the efficiencies can be observed for the recuperated case. With the exception of methane, all fluids lead to an improvement in efficiency, which tends to increase with higher mole fractions. Particularly noticeable is propane with an increase of about 4% at a mole fraction of 40%, see Figure 4d. In the group of aromatics, alcohols, ethers, and naphtenics, only small changes can be noted for both cycles. The reversal of efficiency trends when comparing the simple with the recuperated cycle also occurs for these substances. Similar to the

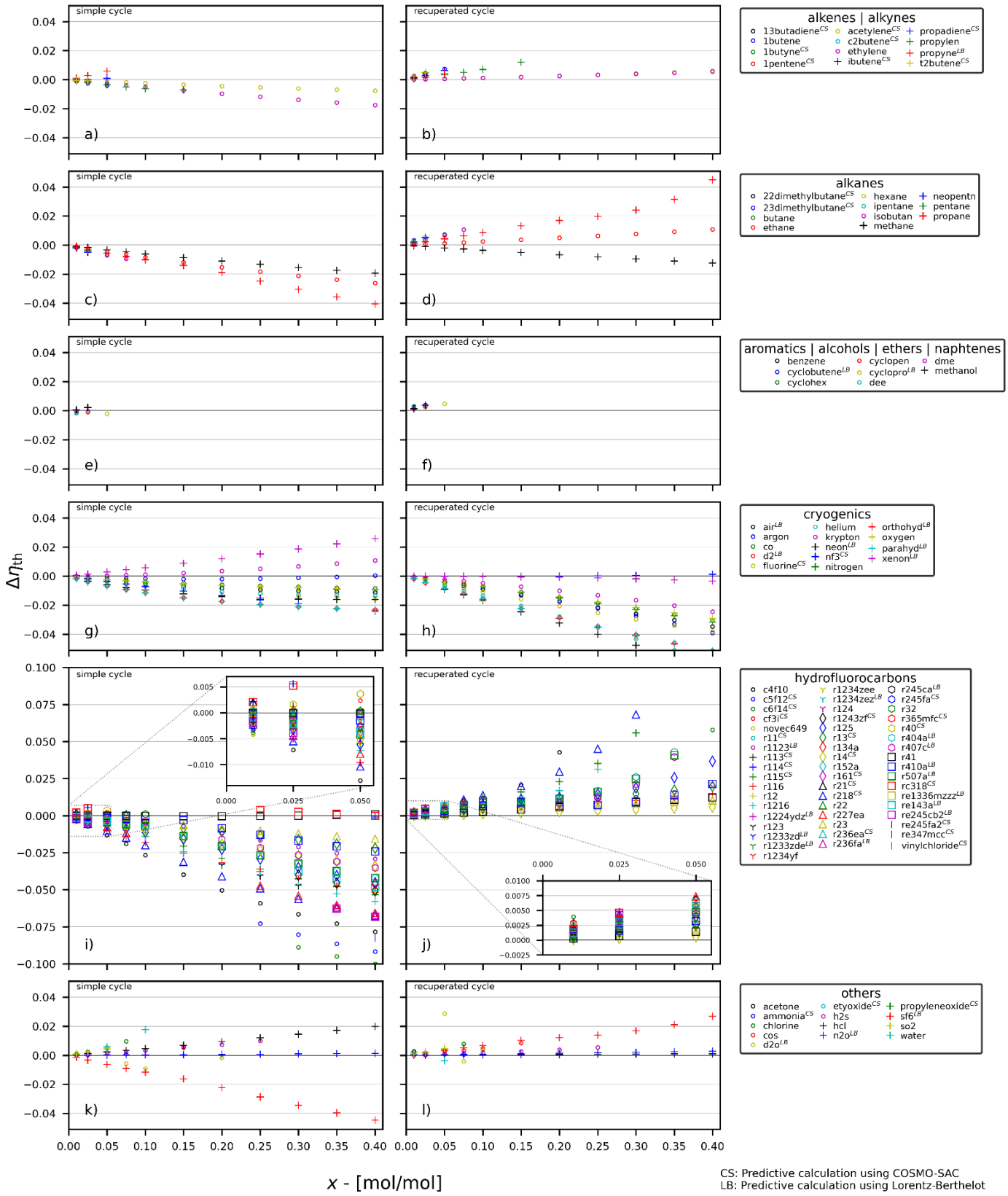

Figure 4: Efficiency change of the considered mixtures compared to cycles with pure CO_2 as working fluid for the minimum process temperature $\vartheta_{low} = 40$ °C and all other boundary conditions as given in Table 1.

previously discussed substances, most of the substances in this group that have led to a negative effect in the simple cycle cause positive changes in the recuperated case. However, methanol is exceptional, as it slightly increases the efficiency in both cases for low concentrations. As indicated by the absence of plot points for higher mole fractions in Figure 4e and f, another significant aspect of this group of fluids is a strongly decreasing solubility of the mixing partners with increasing mole fraction. When the solubility limit is reached, more than one fluid phase is present at some of the state points. Consequently, the corresponding results were discarded during the pre-selection process. Contrary to the groups mentioned before, a distinct improvement of the efficiency for the simple cycle can be found in the group of cryogenic fluids for several species. As shown in Figure 4g, the addition of krypton causes an improvement in efficiency of approx. 1% at a molar fraction of 40%, while the same amount of xenon leads to a calculated increase in efficiency of over 2.5%. An increasing efficiency with increasing mole fractions can also be assumed for argon at mole fractions of argon higher than 40%, which, however, have not been investigated in this study. At a closer look, it is remarkable that all three mentioned fluids are from the group of noble gases. Furthermore, for xenon, krypton, and argon, the increase in efficiency correlates with the respective ordinal number. Figure 5 shows a separate comparison of the results for the noble gases. For the binary mixture of xenon + CO_2, Lorentz-Berthelot combining rules (LB) have been applied as neither an adjusted mixture model is available nor a σ-profile for xenon in order to apply COSMO-SAC are available. In order to estimate the validity of the results for xenon regarding the efficiency calculations, results for krypton calculated with the multi-fluid mixture model with adjusted parameters have been compared to results for krypton using the LB-model. Figure 5 shows that for the binary mixture of CO_2 + krypton the deviations of these models in calculated thermal efficiencies for the simple cylce are rather small. It can therefore be assumed that the LB-model also provides reasonable results for CO_2 + xenon. Looking at the recuperated case in Figure 4h,

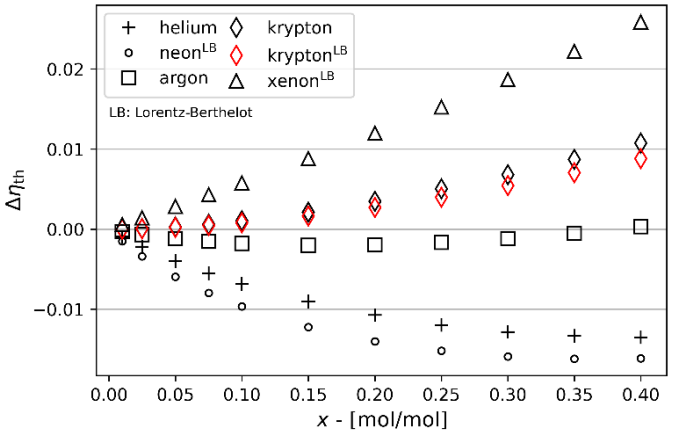

Figure 5: Comparison of the difference in efficiencies of the simple cycle model for mixtures with various noble gases from the efficiency for pure CO_2.

it can be seen that the efficiency of xenon shows only a slight downward trend, instead of decreasing rapidly as many of the other fluids in the cryogenics group. For krypton, however, the reversal of the trend is more apparent, i.e., for the simple cycle the efficiency increases with increasing mole fractions of krypton and for the recuperated cycle the efficiency decreases. Almost all other fluids in this group lead to a loss of efficiency for both cycle architectures further decreasing with higher mixing ratios. Contrarily, in the group of hydrofluorocarbons, see Figure 4i and j, the reversal of the trends is again evident for most fluids. Especially at higher mole fractions of the additives, see for example the addition of R-115, R-125 or R-218, a distinct reduction in efficiency for the simple cycle and on the contrary a noticeable increase of the efficiency for the recuperated cycle is apparent. Apart from this, several mixtures with low mole fractions of the additive can be found, which slightly improve the efficiency for both cycle architectures. As can be seen in the detailed views of Figure 4i and Figure 4j, this applies, for example, to R-114 and RC-318 for mole fractions of 2.5% and to R-40 and CF_3I for mole fractions up to 5%. For R-32, our model could not confirm the potential improvements in simple cycle efficiencies previously reported by Baik and Lee [8]. When comparing the two cycles in this group, it is also noticeable that the recuperated case contains a significantly lower number of fluids than the simple cycle, which is a result of pinch point violations in the recuperator and discarding of all of the mixtures for which this violations occurred. By taking a closer look at the results for the simple cycle, RC-318 yields phases splits at the state points of the cycle between 2.5% and 25%, see Figure 4i. Regarding the results of the last group (“others”) in Figure 4k and Figure 4l, most substances show positive changes in efficiency for both cycle layouts. Especially by adding hydrochloric acid (HCl) or water an increase up to 2% has been calculated for the simple cycle. While the addition of water has no positive effect in the recuperated case, mainly the addition of hydrogen sulfide (H_2S) or carbonyl sulfide (COS) leads to better efficiencies in both cases. Sulfur hexafluoride (SF_6) behaves differently than the other fluids in this group as it shows a distinct improvement in the recuperated case and a decrease in the simple cycle. Compared to propane (see and Figure 4c and d), there is a remarkable similarity in the behavior. With increasing mole fraction, both fluids lead to a strong reduction of efficiency in the simple cycle, whereas under the aforementioned keyword “trend reversal”, an even strong improvement can be observed in the recuperated case. However, note that CO_2 + SF_6 has been modeled with the simple LB-model as neither a model with adjusted parameters nor a σ-profile for SF_6 in order to use COSMO-SAC are available. Regarding the results for heavy water (D_2O), a sudden change in efficiency occurs in the recuperated case when comparing the molar fractions of 5% and 7.5%. For CO_2 + water an adjusted mixture model exists [24] whereas for CO_2 + heavy water the LB-model had to be used. As there is a lack of similarity between the results for normal water and heavy water, it is assumed that the sudden changes stem from erroneous behavior of the simple predictive mixture model. In order to carry out a representative investigation of several

influences on the efficiency, five promising mixing partners were selected for a more detailed investigation. The selected fluids are listed in Table 2 including their largest influence on the efficiencies of both types of cycles.

Table 2: Selection of promising mixing partners for a more detailed analysis.

Name	Chemical symbol	Mixing Model	$\Delta\eta_{\mathrm{th,max}}$ Simple cycle	$\Delta\eta_{\mathrm{th,max}}$ Recuperated cycle
Carbonyl sulfide	COS	Adjusted	$\approx +1.0\%$	$\approx +0.5\%$
Krypton	Kr	Adjusted	$\approx +1.2\%$	$\approx -2.2\%$
Propane	C_3H_8	Adjusted	$\approx -4.2\%$	$\approx +4.2\%$
Sulfur hexafluoride	SF_6	LB	$\approx -4.2\%$	$\approx +2.3\%$
Xenon	Xe	LB	$\approx +2.2\%$	$\approx -0.25\%$

Based on the previously mentioned performance in the recuperated case, propane and SF_6 were selected. Due to the significant increase in efficiency in the simple cycle, the noble gases xenon and krypton have also been selected. From the last group, COS was selected for a more detailed examination as it shows increasing efficiencies with increasing mole fractions for both cycle process architectures. In the same group, similar efficiency changes but with a smaller impact in the recuperated case can be seen when adding H_2S. Furthermore, significant efficiency increases were also observed for several hydrofluorocarbons for the recuperated cycle. However, since the majority of the species with significant impact on efficiency have high global warming potentials (GWP) and/or ozone depletion potentials (ODP) (e.g. R-218, R-115, RC-318, R-404A) [93,94], these species were not considered further. Additionally, also water and HCl were not further investigated, despite significant positive effects on efficiency, because HCl is rather harmful and many mixture compositions of CO_2 + water lead to phase splits. For the evaluation of the influencing factors causing the efficiency variations, Figure 6 shows the process cycles in the h-s diagram for several concentrations of the selected mixing partners. Additionally, a representation of the changes in the enthalpy differences (compared to the cycle with pure CO_2) is given by bar charts. In these charts, Δh_{C} stands for the compression work, Δh_{R} for the recuperated heat (recuperated case, points 2-3), Δh_{H} denotes the heat added in the heater (recuperated case, points 3-4), Δh_{T} denotes the enthalpy difference in the turbine and $\Delta h_{Q,\mathrm{tot}}$ stands for the total heat added between the compressor exit and the turbine inlet. Beginning from the top with xenon it can be seen that with increasing mole fractions the position of the isobars remains almost unaffected. However, it is more apparent that the upper end of the cycle, even though the turbine inlet temperature TIT remains constant, moves towards lower enthalpy values with increasing molar fractions of xenon. In this way, the amount of total heat $\Delta h_{Q,\mathrm{tot}}$ reduces. Thus, the efficiency of the simple cycle increases by compensating the slight deteriorations regarding the enthalpy differences of the compressor Δh_{C} and the turbine Δh_{T} with a distinct decrease of the added heat. At the same time, the heat transferred in the recuperator Δh_{R} is reduced,

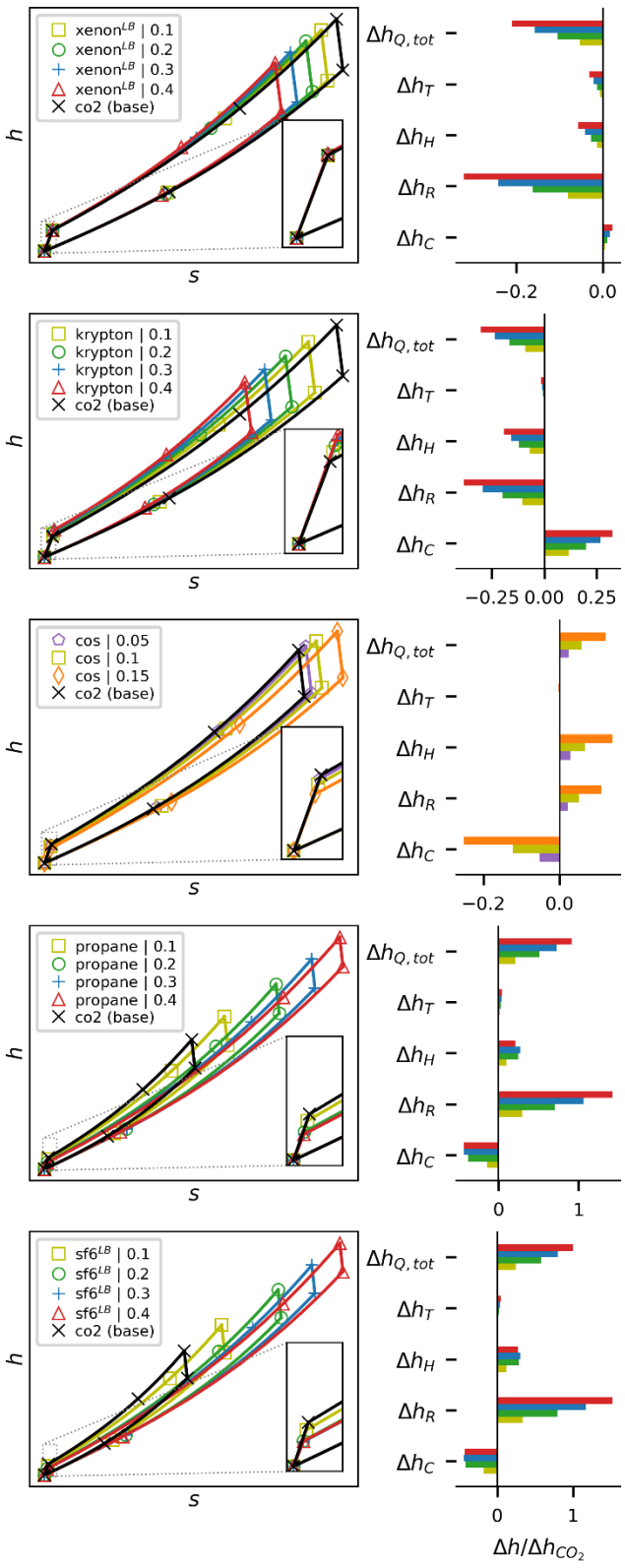

Figure 6: Effects of selected mixtures on the shape and location of the process in the h-s diagram and the differences in enthalpies in the components compared to the cycle with pure CO_2.

which in the recuperated case cancels out the positive increase in efficiency. Similar results are obtained for krypton. The resulting relative reduction of $\Delta h_{Q,\mathrm{tot}}$ and Δh_{H} is even greater than for xenon but gets compensated by a significant increase of Δh_{C}, clearly reducing the increase in efficiency of the simple cycle compared to xenon. Again, the same effects as for xenon lead to a more significant drop in the performance of the recuperated case. Contrary to the two noble gases, the plots for COS show a slight decrease of the slopes of the isobars in the *h-s* diagram with increasing mole fractions. Additionally, higher amounts of COS lead to higher enthalpy values for the upper temperature level resulting in an increase of heat to be added, as can be seen for $\Delta h_{Q,\mathrm{tot}}$ and Δh_{H} in the bar chart. While the turbine output Δh_{T} remains almost the same, the compression work Δh_{C} reduces significantly, which results in the positive change in efficiency for both cycle architectures as shown in Figure 4. Furthermore, the enthalpy differences change unevenly with increasing mole fractions, see Figure 6. Using the example of the enthalpy difference in the compressor Δh_{C}, the change from a mole fraction of 0.10 to 0.15 is significantly greater than from 0.05 to 0.10. By comparing the plots for propane and SF_6 it can be seen that both the shape of the cycles as well as the bar charts representing the relative enthalpy differences are almost identical for both fluids. The slopes of the isobars decrease noticeably with increasing concentrations for both fluids. The compressor work Δh_{C} is reduced by up to approximately 40% while the enthalpy difference in the turbine remains nearly unaffected. The bar charts show that the total heat input $\Delta h_{Q,\mathrm{tot}}$ needs to be more than doubled for higher mole fractions. As the increase in added heat significantly exceeds the aforementioned savings of compressor work, this mainly causes the previously discussed deterioration of the simple cycle efficiency for both fluids. Regarding the recuperated cases, it is noticeable that the amount of heat available for recuperation increases even more than the amount of total heat needed. For the highest mole fractions, the recuperated heat increases to approximately 140% of the recuperated heat when using pure CO_2. Furthermore, it is apparent that the recuperated heat increases significantly more with the mole fraction of propane or SF_6 than the heat Δh_{H} that needs to be added in the heater.

Figure 7 shows critical curves as well as phase envelopes for some of the studied binary mixtures. The algorithms for calculating phase equilibria and critical points, which are implemented in TREND 4.0, are described in refs. [90,95]. As can be seen in the uppermost subplot, adding xenon hardly influences the form and shape of the phase boundaries compared to pure CO_2. The critical point itself shifts with higher mole fractions to lower temperatures and lower pressures approaching the critical point of xenon. Compared to the other substances studied, the critical point of xenon is relatively close to the critical point of CO_2. This explains the previously discussed similarity regarding the cold end of the cycle and the isobars. By contrast, adding krypton to CO_2 clearly shifts the position of the dew and bubble line. Regarding the temperature, the critical point moves to lower values with higher concentrations of

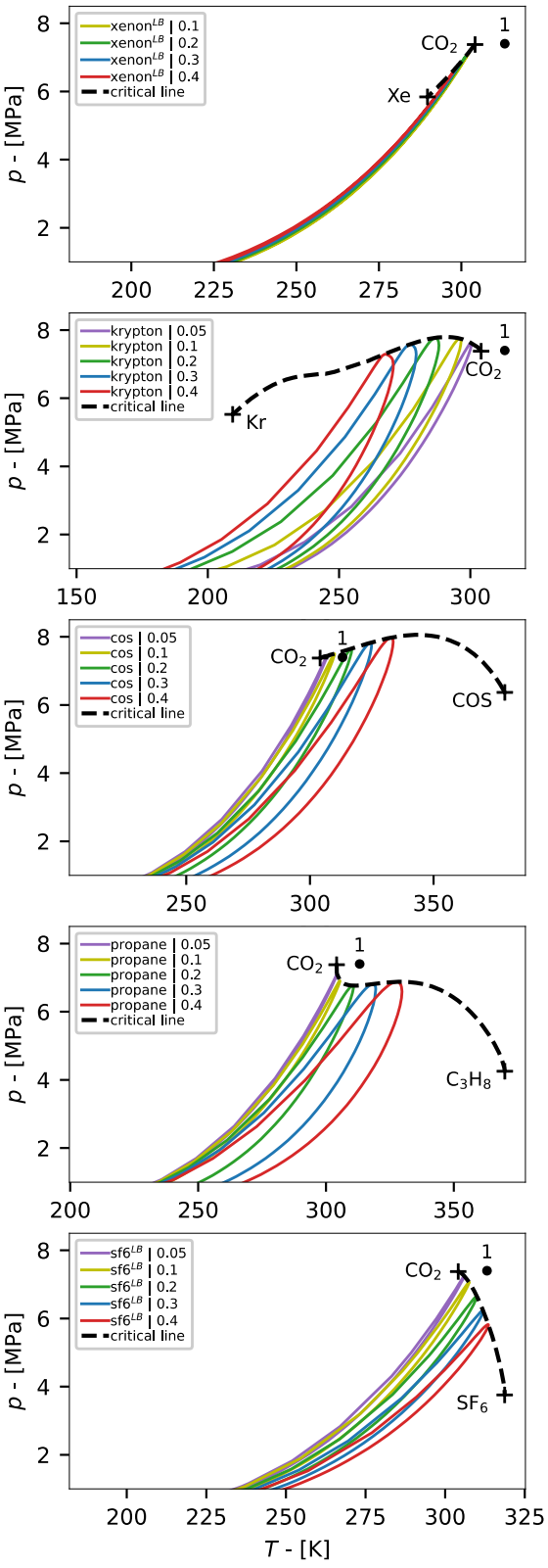

Figure 7: Critical curves and phase envelopes for the studied mixtures. Point 1 marks the CIT used in the screening.

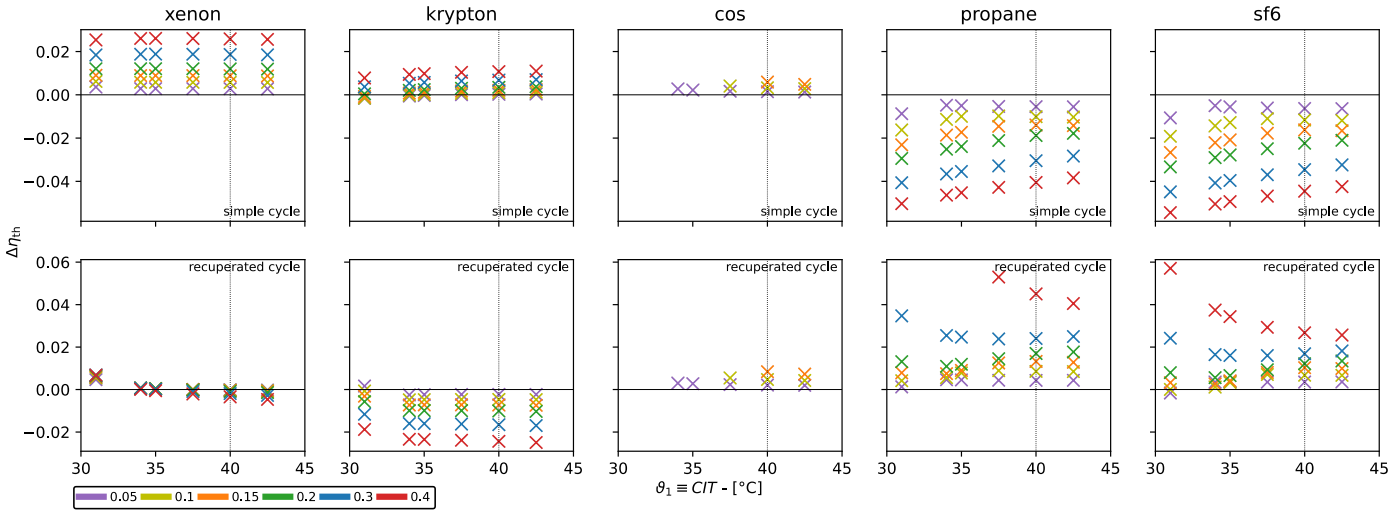

Figure 8: Temperature dependence of the change in efficiency for the selected mixtures.

krypton in CO_2. The critical pressure on the other hand increases up to a molar fraction of approximately 0.2 and then reduces with higher concentrations. In contrast to the other fluids in Figure 7, the addition of COS initially changes the critical point towards higher pressures and higher temperatures, so that it gets gradually closer to the inlet conditions of the compressor. This results in a reduction of the compressor work shown in Figure 6. From a molar fraction of approx. 0.17, both the critical pressure and critical temperature are higher than the pressure and temperature at the compressor inlet, respectively. Thus, these points were rejected because of the presence of two fluid phases in the pre-selection. For both propane and SF_6, higher concentrations result in a change of the critical point to lower pressures and higher temperatures. Nevertheless, in contrast to the *h-s* diagrams in Figure 6, Figure 7 shows considerable differences for both fluids. Note that the critical curves of SF_6 and Xenon have been calculated with the simple LB-model and therefore larger deviations from the real fluid behavior may occur, see, e.g., ref. [12,13,96,97]. For propane, the calculated critical pressure drops steeply up to a molar fraction of about 0.2. Subsequently, the pressure slightly increases up to a molar fraction of 0.4 and then drops sharply with higher concentrations. On the other hand, for SF_6 the calculated critical pressure shows an immediate and persistent decrease. Thus, the critical temperature of propane + CO_2 mixtures increases to higher values than the critical temperature of SF_6 + CO_2 mixtures investigated in this study.

Applying the boundary conditions defined in Table 1, Figure 8 shows the change in thermal efficiency for different concentrations of the selected mixtures (see Table 2) over the entire range of compressor inlet temperatures (CIT). For the two noble gases xenon and krypton, the change in efficiency calculated for the simple cycle remains almost constant for all concentrations over the entire temperature range. Only krypton shows a slight drop at lower temperatures. It is remarkable that xenon shows hardly any deterioration of the efficiency against pure CO_2 at any time. In the recuperated case, both fluids show a small increase in efficiency towards lower temperatures. For COS, the efficiencies compared to pure CO_2 increase slightly with decreasing temperatures for both cycles. However, due to the absence of the corresponding points in the plot, it is noticeable that the mixture decomposes into more than one phase both at lower temperatures and at high concentrations of COS in CO_2. Even with a comparatively low molar fraction of 0.05, the entire temperature range cannot be covered without several fluid phases being present in one or more cycle points. This is consistent with the previously discussed shift of the critical point to higher pressures and temperatures at higher concentrations. Equivalently to Figure 6, propane and SF_6 also show almost the same behavior in Figure 8. In contrast to SF_6, however, propane shows a pinch-point violation in the recuperated case at high concentrations. Apart from this, both fluids show a significant decrease in efficiency (compared to pure CO_2) of the simple cycle at lower temperatures across all concentrations. Despite different boundary conditions, the trend for SF_6 is consistent with the results previously reported by Baik and Lee [8]. In contrast to the simple cycle, for both fluids this effect is mostly reversed in the recuperated case. For lower temperatures, higher efficiency increases are achieved with a steeper decline for higher concentrations. Only at low concentrations, a reduction of the increase in efficiency to low temperatures can be seen.

CONCLUSIONS

In this work, the potential for increasing the thermal efficiency by adding additives to pure CO_2 was evaluated based on an exemplary application of a sCO_2 cycle. Using predictive mixing models as well as accurate multi-fluid mixture models with adjusted parameters, a comprehensive screening for 135 fluids was performed for two different cycle layouts. From these results, five potential mixture candidates were chosen and investigated in detail. Within this selection, efficiency increases of more than 4% compared to a cycle with pure CO_2 and the same

boundary conditions are predicted. For simple cycle applications, the use of the noble gases xenon and krypton has been found to be particularly interesting. Especially xenon offers a noticeable efficiency increase over a wide temperature range with similar cycle properties compared to pure CO_2. In the recuperated case, the largest increases in thermal efficiency have been calculated for SF_6 and propane, when omitting the hydrofluorocarbons having a large GWP and/or ODP. However, upon closer investigation it was found that a large amount of heat would need to be recuperated when using the binary mixtures of CO_2 with propane or SF_6 in a recuperated cycle. This would lead to a large size of the heat exchanger and therefore is most likely not economically feasible.

Since this study was mainly concerned with a theoretical screening of potential additives to CO_2 in order to increase the thermal efficiency, in a further step additional investigations concerning the selected mixtures would be necessary. For example the thermal stability of additives and chemical reactions should be investigated, as studies show that SF_6 and COS possibly decompose into other substances at temperatures close to or below the maximum temperature of the cycles investigated in this study [98–100].

In general, it has been shown in this work that the increases in efficiency can be attributed to different effects depending on the fluid, the molar composition of the mixture, and the boundary conditions. All of these parameters have an influence on the compression enthalpy, amount of heat to be added to the cycle and heat available for recuperation, which directly influence the thermal efficiency. It has been demonstrated that the critical point can be shifted within certain limits to lower as well as to higher pressures and temperatures when adding a suitable mixing partner. However, special care needs to be taken in order to avoid multi-phase flows in sensitive components, as adding a substance might lead to phase splits as discussed for example for COS. This all requires the mixture to be adapted to the respective application.

This work was restricted to predicting the efficiency of two cycle configurations using binary mixtures of CO_2 with other substances for which multi-parameter equations of state are available. Future work will focus on the application of this method to more complex cycle architectures and variable boundary conditions. Furthermore, the amount of mixtures investigated could be significantly increased by considering multi-component mixtures and by extending the database of the pure fluids by on the one hand using simpler equations of state for the pure fluids (e.g. cubic equations of state) and on the other hand perform COSMO-calculations for missing substances.

NOMENCLATURE

Symbols

A	molecular surface area (Å^2)
A_{ES}	constant of COSMO-SAC (kcal Å^4 mol^{-1} e^{-2})
b	co-volume (m^3 mol^{-1})
B_{ES}	constant of COSMO-SAC (kcal Å^4 K^2 mol^{-1} e^{-2})
c_{hb}	constant of COSMO-SAC (kcal Å^4 mol^{-1} e^{-2})
∂	partial derivative
F	parameter of the departure function
g	molar Gibbs energy (J mol^{-1})
i	index of summation
j	index of summation
n	number of standard surface segments of a molecule
N	number of components in the mixture
p	pressure (Pa)
$p(\sigma)$	sigma-profile
R	universal gas constant (J mol^{-1} K^{-1})
T	temperature (K)
x	mole fraction
$\vec{x}$	vector of mole fractions

Greek symbols

α	dimensionless Helmholtz energy
β	model parameter
δ	reduced density
γ	model parameter
Γ	Segment activity coefficient
η	Efficiency
ϑ	temperature (°C)
ρ	molar density (mol m^{-3})
σ	screening charge density (e Å^{-2})
τ	reduced temperature (-)

Subscripts

c	property at the critical point
ES	electrostatic
GE	property calculated from an excess Gibbs energy model
hb	hydrogen-bonding
i	property of component i
j	property of component j
o	property of a pure fluid
r	reducing property
s	property at saturation (at vapor-liquid equilibrium)
T	related to the turbine
C	related to the compressor
R	related to the recuperator
tot	total (amount)
ref	property at reference pressure

Superscripts

0	ideal gas property
E	excess property
L	property of a liquid phase
r	residual property

Chemical Formulas

CO_2	carbon dioxide
N_2O_4	dinitrogen tetroxide
SF_6	sulfur hexafluoride
$TiCl_4$	titanium(IV) chloride

Abbreviations

CIT	Compressor inlet temperature
COSMO	Conductor-like screening model
COSMO-RS	Conductor-like screening model for real solvents
COSMO-SAC	Conductor-like screening model segment activity coefficients
CS	The binary mixture was modeled predictively with the combination of the multi-fluid mixture model with COSMO-SAC
GWP	Global warming potential
LB	The binary mixture was modeled predictively using Lorentz-Berthelot combining rules
ODP	Ozone depletion potential
PR	Peng-Robinson equation of state
SAFT	Statistical associating fluid theory
SRK	Soave-Redlich-Kwong equation of state
TIT	Turbine inlet temperature

ACKNOWLEDGEMENTS

This work was carried out within the Supercritical Carbon Dioxide-Lab (suCOO-Lab) of the School of Engineering Sciences of TU Dresden. The authors want to thank the School of Engineering Sciences of TU Dresden for partial funding of the presented results.

REFERENCES

[1] Y. Ahn, S.J. Bae, M. Kim, S.K. Cho, S. Baik, J.I. Lee, J.E. Cha, Review of supercritical CO2 power cycle technology and current status of research and development, Nucl. Eng. Technol. 47 (2015) 647–661. https://doi.org/10.1016/j.net.2015.06.009.

[2] C. Geng, Y. Shao, W. Zhong, X. Liu, Thermodynamic Analysis of Supercritical CO_2 Power Cycle with Fluidized Bed Coal Combustion, Journal of Combustion. 2018 (2018) 1–9. https://doi.org/10.1155/2018/6963292.

[3] U. Gampe, J. Henoch, G. Gerbeth, F. Hannemann, S. Rath, U. Hampel, S. Glos, Concept and preliminary design of a 600 °C+ sCO2 test facility, in: Proceedings of the 2nd European SCO2 Conference 2018, Essen, Germany, 2018. https://doi.org/10.17185/duepublico/46084.

[4] J. Yin, Q. Zheng, Z. Peng, X. Zhang, Review of supercritical CO_2 power cycles integrated with CSP, Int J Energy Res. 44 (2020) 1337–1369. https://doi.org/10.1002/er.4909.

[5] V. Dostal, P. Hejzlar, M.J. Driscoll, The Supercritical Carbon Dioxide Power Cycle: Comparison to Other Advanced Power Cycles, Nuclear Technology. 154 (2006) 283–301. https://doi.org/10.13182/NT06-A3734.

[6] O. Kizilkan, Performance assessment of steam Rankine cycle and sCO_2 Brayton cycle for waste heat recovery in a cement plant: A comparative study for supercritical fluids, Int J Energy Res. (2020) er.5138. https://doi.org/10.1002/er.5138.

[7] S. Glos, M. Wechsung, R. Wagner, A. Heidenhof, D. Schlehuber, Evaluation of sCO2 power cycles for direct and waste heat applications, (2018). https://doi.org/10.17185/DUEPUBLICO/46082.

[8] S. Baik, J.I. Lee, Preliminary Study of Supercritical CO2 Mixed With Gases for Power Cycle in Warm Environments, in: Volume 9: Oil and Gas Applications; Supercritical CO2 Power Cycles; Wind Energy, American Society of Mechanical Engineers, Oslo, Norway, 2018: p. V009T38A017. https://doi.org/10.1115/GT2018-76386.

[9] M. Binotti, C.M. Invernizzi, P. Iora, G. Manzolini, Dinitrogen tetroxide and carbon dioxide mixtures as working fluids in solar tower plants, Solar Energy. 181 (2019) 203–213. https://doi.org/10.1016/j.solener.2019.01.079.

[10] M. Binotti, G. Di Marcoberardino, P. Iora, C.M. Invernizzi, G. Manzolini, Supercritical carbon dioxide/alternative fluid blends for efficiency upgrade of solar power plant, Proceedings of the 3rd European Supercritical CO2 Conference. (2019). https://doi.org/10.17185/DUEPUBLICO/48892.

[11] G. Manzolini, M. Binotti, D. Bonalumi, C. Invernizzi, P. Iora, CO_2 mixtures as innovative working fluid in power cycles applied to solar plants. Techno-economic assessment, Solar Energy. 181 (2019) 530–544. https://doi.org/10.1016/j.solener.2019.01.015.

[12] A. Jäger, I.H. Bell, C. Breitkopf, A theoretically based departure function for multi-fluid mixture models, Fluid Phase Equilib. 469 (2018) 56–69. https://doi.org/10.1016/j.fluid.2018.04.015.

[13] A. Jäger, E. Mickoleit, C. Breitkopf, A Combination of Multi-Fluid Mixture Models with COSMO-SAC, Fluid Phase Equilib. 476 (2018) 147–156. https://doi.org/10.1016/j.fluid.2018.08.004.

[14] R. Span, W. Wagner, A New Equation of State for Carbon Dioxide Covering the Fluid Region from the Triple-Point Temperature to 1100 K at Pressures up to 800 MPa, J. Phys. Chem. Ref. Data. 25 (1996) 1509–1596. https://doi.org/10.1063/1.555991.

[15] A. Fredenslund, R.L. Jones, J.M. Prausnitz, Group-Contribution Estimation of Activity Coefficients in Nonideal Liquid Mixtures, AIChE J. 21 (1975) 1086–1099.

[16] S.-T. Lin, S.I. Sandler, A Priori Phase Equilibrium Prediction from a Segment Contribution Solvation Model, Ind. Eng. Chem. Res. 41 (2002) 899–913. https://doi.org/10.1021/ie001047w.

[17] S.-T. Lin, S.I. Sandler, A Priori Phase Equilibrium Prediction from a Segment Contribution Solvation Model. - Additions and Corrections, Ind. Eng. Chem. Res. 43 (2004) 1322–1322. https://doi.org/10.1021/ie0308689.

[18] C.-M. Hsieh, S.I. Sandler, S.-T. Lin, Improvements of COSMO-SAC for vapor–liquid and liquid–liquid equilibrium predictions, Fluid Phase Equilibria. 297 (2010) 90–97. https://doi.org/10.1016/j.fluid.2010.06.011.

[19] E. Mickoleit, A. Jäger, C. Breitkopf, Carrier-Fluid Screening for a Three-Phase Sublimation Refrigeration Cycle with CO_2 Using Reference Equations of State and

COSMO-SAC, J. Chem. Eng. Data. (2019) 1124–1134. https://doi.org/10.1021/acs.jced.9b00514.
[20] E. Mickoleit, C. Breitkopf, A. Jäger, Influence of Equations of State and Mixture Models on the Design of a Refrigeration Process, Int. J. Refrig. 121 (2021) 193–205. https://doi.org/10.1016/j.ijrefrig.2020.10.017.
[21] E.W. Lemmon, R. Tillner-Roth, A Helmholtz Energy Equation of State for Calculating the Thermodynamic Properties of Fluid Mixtures, Fluid Phase Equilib. 165 (1999) 1–21.
[22] O. Kunz, R. Klimeck, W. Wagner, M. Jaeschke, The Gerg-2004 Wide Range Equation of State for Natural Gases and Other Mixtures GERG TM15 2007, VDI-Verl., Düsseldorf, Germany, 2007.
[23] O. Kunz, W. Wagner, The GERG-2008 Wide-Range Equation of State for Natural Gases and Other Mixtures: An Expansion of GERG-2004, J. Chem. Eng. Data. 57 (2012) 3032–3091. https://doi.org/10.1021/je300655b.
[24] J. Gernert, R. Span, EOS–CG: A Helmholtz energy mixture model for humid gases and CCS mixtures, J. Chem. Thermodyn. 93 (2016) 274–293. https://doi.org/10.1016/j.jct.2015.05.015.
[25] S. Herrig, New Helmholtz-energy equations of state for pure fluids and CCS-relevant mixtures, Dissertation, Ruhr-Universität Bochum, 2018.
[26] R. Klimeck, Entwicklung einer Fundamentalgleichung für Erdgase für das Gas- und Flüssigkeitsgebiet sowie das Phasengleichgewicht, Dissertation, Ruhr-Universität Bochum, 2000.
[27] I.H. Bell, A. Jäger, Helmholtz Energy Transformations of Common Cubic Equations of State for Use with Pure Fluids and Mixtures, J Res Natl Inst Stan. 121 (2016) 238–263. https://doi.org/10.6028/jres.121.011.
[28] O. Redlich, J.N.S. Kwong, On the Thermodynamics of Solutions. V. An Equation of State. Fugacities of Gaseous Solutions., Chem. Rev. 44 (1949) 233–244.
[29] G. Soave, Equilibrium Constants from a Modified Redlich-Kwong Equation of State, Chem. Eng. Sci. 27 (1972) 1197–1203. https://doi.org/10.1016/0009-2509(72)80096-4.
[30] D.-Y. Peng, D.B. Robinson, A New Two-Constant Equation of State, Ind. Eng. Chem. Fund. 15 (1976) 59–64. https://doi.org/10.1021/i160057a011.
[31] E.W. Lemmon, I.H. Bell, M.L. Huber, M.O. McLinden, REFPROP, NIST Standard Reference Database 23 Version 10.0, Boulder, USA, 2018.
[32] E.W. Lemmon, E.C. Ihmels, Thermodynamic properties of the butenes: Part II. Short fundamental equations of state, Fluid Phase Equilib. 228–229 (2005) 173–187. https://doi.org/10.1016/j.fluid.2004.09.004.
[33] A. Polt, B. Platzer, G. Maurer, Parameter der Thermischen Zustandsgleichung von Bender für 14 Mehratomige Reine Stoffe, Chem. Tech. (Leipzig). 44 (1992) 216–224.
[34] E.W. Lemmon, R. Span, Short Fundamental Equations of State for 20 Industrial Fluids, J. Chem. Eng. Data. 51 (2006) 785–850. https://doi.org/10.1021/je050186n.
[35] M. Thol, E.W. Lemmon, R. Span, Equation of State for Benzene for Temperatures from the Melting Line up to 725 K with Pressures up to 500 MPa, High Temp. - High Pressures. 41 (2012) 81–97.
[36] D. Bücker, W. Wagner, Reference Equations of State for the Thermodynamic Properties of Fluid Phase n-Butane and Isobutane, J. Phys. Chem. Ref. Data. 35 (2006) 929–1019. https://doi.org/10.1063/1.1901687.
[37] U. Setzmann, W. Wagner, A New Equation of State and Tables of Thermodynamic Properties for Methane Covering the Range from the Melting Line to 625 K at Pressures up to 100 MPa, J. Phys. Chem. Ref. Data. 20 (1991) 1061–1155. https://doi.org/10.1063/1.555898.
[38] E.W. Lemmon, R. Span, Thermodynamic Properties of R-227ea, R-365mfc, R-115, and R-13I1, J. Chem. Eng. Data. 60 (2015) 3745–3758. https://doi.org/10.1021/acs.jced.5b00684.
[39] Y. Zhou, J. Liu, S.G. Penoncello, E.W. Lemmon, An Equation of State for the Thermodynamic Properties of Cyclohexane, J. Phys. Chem. Ref. Data. 43 (2014) 043105. https://doi.org/10.1063/1.4900538.
[40] H. Gedanitz, M.J. Davila, E.W. Lemmon, Speed of Sound Measurements and a Fundamental Equation of State for Cyclopentane, J. Chem. Eng. Data. 60 (2015) 1331–1337. https://doi.org/10.1021/je5010164.
[41] K.M. de Reuck, R.J.B. Craven, Methanol, International Thermodynamic Tables of the Fluid State - 12, IUPAC, Blackwell Scientific Publications, London, 1993.
[42] E.W. Lemmon, R.T. Jacobsen, S.G. Penoncello, D.G. Friend, Thermodynamic Properties of Air and Mixtures of Nitrogen, Argon, and Oxygen From 60 to 2000 K at Pressures to 2000 MPa, J. Phys. Chem. Ref. Data. 29 (2000) 331–385. https://doi.org/10.1063/1.1285884.
[43] C. Tegeler, R. Span, W. Wagner, A New Equation of State for Argon Covering the Fluid Region for Temperatures from the Melting Line to 700 K at Pressures up to 1000 MPa, J. Phys. Chem. Ref. Data. 28 (1999) 779–850.
[44] I.A. Richardson, J.W. Leachman, E.W. Lemmon, Fundamental Equation of State for Deuterium, J. Phys. Chem. Ref. Data. 43 (2014) 013103. https://doi.org/10.1063/1.4864752.
[45] R. Span, E.W. Lemmon, R.T. Jacobsen, W. Wagner, A. Yokozeki, A Reference Equation of State for the Thermodynamic Properties of Nitrogen for Temperatures from 63.151 to 1000 K and Pressures to 2200 MPa, Journal of Physical and Chemical Reference Data. 29 (2000) 1361–1433.
[46] J.W. Leachman, R.T. Jacobsen, S.G. Penoncello, E.W. Lemmon, Fundamental Equations of State for Parahydrogen, Normal Hydrogen, and Orthohydrogen, J. Phys. Chem. Ref. Data. 38 (2009) 721–748. https://doi.org/10.1063/1.3160306.
[47] R. Schmidt, W. Wagner, A New Form of the Equation of State for Pure Substances and Its Application to Oxygen, Fluid Phase Equilibria. 19 (1985) 175–200.

[48] M.O. McLinden, R.A. Perkins, E.W. Lemmon, T.J. Fortin, Thermodynamic Properties of 1,1,1,2,2,4,5,5,5-Nonafluoro-4-(trifluoromethyl)-3-pentanone: Vapor Pressure, (p , ρ, T) Behavior, and Speed of Sound Measurements, and an Equation of State, J. Chem. Eng. Data. 60 (2015) 3646–3659. https://doi.org/10.1021/acs.jced.5b00623.

[49] J. Wu, Y. Zhou, E.W. Lemmon, An Equation of State for the Thermodynamic Properties of Dimethyl Ether, Journal of Physical and Chemical Reference Data. 40 (2011) 023104. https://doi.org/10.1063/1.3582533.

[50] D. Bücker, W. Wagner, A Reference Equation of State for the Thermodynamic Properties of Ethane for Temperatures from the Melting Line to 675 K and Pressures up to 900 MPa, J. Phys. Chem. Ref. Data. 35 (2006) 205–266. https://doi.org/10.1063/1.1859286.

[51] J. Smukala, R. Span, W. Wagner, New Equation of State for Ethylene Covering the Fluid Region for Temperatures From the Melting Line to 450 K at Pressures up to 300 MPa, J. Phys. Chem. Ref. Data. 29 (2000) 1053–1121. https://doi.org/10.1063/1.1329318.

[52] M. Thol, G. Rutkai, A. Köster, M. Kortmann, R. Span, J. Vrabec, Fundamental equation of state for ethylene oxide based on a hybrid dataset, Chem. Eng. Sci. 121 (2015) 87–99. https://doi.org/10.1016/j.ces.2014.07.051.

[53] M. Thol, G. Rutkai, A. Köster, M. Kortmann, R. Span, J. Vrabec, Corrigendum to 'Fundamental equation of state for ethylene oxide based on a hybrid dataset' [Journal of Chemical Engineering Science 121 (2015) 87–99], Chem. Eng. Sci. 134 (2015) 887–890. https://doi.org/10.1016/j.ces.2015.06.020.

[54] K.M. de Reuck, International Thermodynamic Tables of the Fluid State-11 Fluorine, Pergamon Press, Oxford, 1990.

[55] B.A. Younglove, Thermophysical Properties of Fluids. I. Argon, Ethylene, Parahydrogen, Nitrogen, Nitrogen Trifluoride, and Oxygen, J. Phys. Chem. Ref. Data. 11 (1982) 1–11.

[56] E.W. Lemmon, M.O. McLinden, W. Wagner, Thermodynamic Properties of Propane. III. A Reference Equation of State for Temperatures from the Melting Line to 650 K and Pressures up to 1000 MPa, J. Chem. Eng. Data. 54 (2009) 3141–3180. https://doi.org/10.1021/je900217v.

[57] R.T. Jacobsen, S.G. Penoncello, E.W. Lemmon, A fundamental equation for trichlorofluoromethane (R-11), Fluid Phase Equilib. 80 (1992) 45–56. https://doi.org/10.1016/0378-3812(92)87054-Q.

[58] V. Marx, A. Pruß, W. Wagner, Neue Zustandsgleichungen fuer R 12, R 22, R 11 und R 113. Beschreibung des thermodynamishchen Zustandsverhaltens bei Temperaturen bis 525 K und Druecken bis 200 MPa, VDI Verlag, Düsseldorf, 1992.

[59] J.W. Magee, S.L. Outcalt, J.F. Ely, Molar Heat Capacity Cv, Vapor Pressure, and (p, ρ, T) Measurements from 92 to 350 K at Pressures to 35 MPa and a New Equation of State for Chlorotrifluoromethane (R13), Int. J. Thermophys. 21 (2000) 1097–1121. https://doi.org/10.1023/A:1026446004383.

[60] B. Platzer, A. Polt, G. Maurer, Thermophysical properties of refrigerants, Springer-Verlag, Berlin; New York, 1990.

[61] S.G. Penoncello, E.W. Lemmon, R.T. Jacobsen, Z. Shan, A Fundamental Equation for Trifluoromethane (R-23), J. Phys. Chem. Ref. Data. 32 (2003) 1473–1499. https://doi.org/10.1063/1.1559671.

[62] R. Tillner-Roth, A. Yokozeki, An International Standard Equation of State for Difluoromethane (R-32) for Temperatures from the Triple Point at 136.34 K to 435 K and Pressures up to 70 MPa, J. Phys. Chem. Ref. Data. 26 (1997) 1273–1328. https://doi.org/10.1063/1.556002.

[63] M. Thol, L. Piazza, R. Span, A New Functional Form for Equations of State for Some Weakly Associating Fluids, Int. J. Thermophys. 35 (2014) 783–811. https://doi.org/10.1007/s10765-014-1633-1.

[64] K. Gao, J. Wu, P. Zhang, E.W. Lemmon, A Helmholtz Energy Equation of State for Sulfur Dioxide, J. Chem. Eng. Data. 61 (2016) 2859–2872. https://doi.org/10.1021/acs.jced.6b00195.

[65] B.A. Younglove, M.O. McLinden, An International Standard Equation of State for the Thermodynamic Properties of Refrigerant 123 (2,2-Dichloro-1,1,1-Trifluoroethane), J. Phys. Chem. Ref. Data. 23 (1994) 731–779. https://doi.org/10.1063/1.555950.

[66] M.E. Mondéjar, M.O. McLinden, E.W. Lemmon, Thermodynamic Properties of *trans* -1-Chloro-3,3,3-trifluoropropene (R1233zd(E)): Vapor Pressure, (p , ρ, T) Behavior, and Speed of Sound Measurements, and Equation of State, J. Chem. Eng. Data. 60 (2015) 2477–2489. https://doi.org/10.1021/acs.jced.5b00348.

[67] M. Richter, M.O. McLinden, E.W. Lemmon, Thermodynamic Properties of 2,3,3,3-Tetrafluoroprop-1-ene (R1234yf): Vapor Pressure and p-ρ-TMeasurements and an Equation of State, J. Chem. Eng. Data. 56 (2011) 3254–3264.

[68] M. Thol, E.W. Lemmon, Equation of State for the Thermodynamic Properties of *trans*-1,3,3,3-Tetrafluoropropene [R-1234ze(E)], Int J Thermophys. 37:28 (2016) 1–16.

[69] E.W. Lemmon, R.T. Jacobsen, A New Functional Form and New Fitting Techniques for Equations of State with Application to Pentafluoroethane (HFC-125), J. Phys. Chem. Ref. Data. 34 (2005) 69–108. https://doi.org/10.1063/1.1797813.

[70] R. Tillner-Roth, H.D. Baehr, An International Standard Formulation for the Thermodynamic Properties of 1,1,1,2-Tetrafluoroethane (HFC-134a) for Temperatures from 170 K to 455 K and Pressures up to 70 MPa, J. Phys. Chem. Ref. Data. 23 (1994) 657–729. https://doi.org/10.1063/1.555958.

[71] S.L. Outcalt, M.O. McLinden, A Modified Benedict–Webb–Rubin Equation of State for the Thermodynamic Properties of R152a (1,1-difluoroethane), J. Phys. Chem.

Ref. Data. 25 (1996) 605–636. https://doi.org/10.1063/1.555979.
[72] H. Qi, D. Fang, K. Gao, X. Meng, J. Wu, Compressed Liquid Densities and Helmholtz Energy Equation of State for Fluoroethane (R161), Int. J. Thermophys. 37 (2016). https://doi.org/10.1007/s10765-016-2061-1.
[73] X. Rui, J. Pan, Y. Wang, An equation of state for the thermodynamic properties of 1,1,1,2,3,3-hexafluoropropane (R236ea), Fluid Phase Equilib. 341 (2013) 78–85. https://doi.org/10.1016/j.fluid.2012.12.026.
[74] J. Pan, X. Rui, X. Zhao, L. Qiu, An equation of state for the thermodynamic properties of 1,1,1,3,3,3-hexafluoropropane (HFC-236fa), Fluid Phase Equilib. 321 (2012) 10–16. https://doi.org/10.1016/j.fluid.2012.02.012.
[75] Y. Zhou, E.W. Lemmon, Equation of State for the Thermodynamic Properties of 1,1,2,2,3-Pentafluoropropane (R-245ca), Int. J. Thermophys. 37:27 (2016) 1–11. https://doi.org/10.1007/s10765-016-2039-z.
[76] R. Akasaka, Y. Zhou, E.W. Lemmon, A Fundamental Equation of State for 1,1,1,3,3-Pentafluoropropane (R-245fa), J. Phys. Chem. Ref. Data. 44 (2015) 013104.
[77] E.W. Lemmon, Pseudo-Pure Fluid Equations of State for the Refrigerant Blends R-410A, R-404A, R-507A, and R-407C, Int. J. Thermophys. 24 (2003) 991–1006.
[78] S. Herrig, M. Thol, A.H. Harvey, E.W. Lemmon, A Reference Equation of State for Heavy Water, J. Phys. Chem. Ref. Data. 47 (2018) 043102. https://doi.org/10.1063/1.5053993.
[79] M. Thol, F.H. Dubberke, E. Baumhögger, R. Span, J. Vrabec, Speed of Sound Measurements and a Fundamental Equation of State for Hydrogen Chloride, J. Chem. Eng. Data. 63 (2018) 2533–2547. https://doi.org/10.1021/acs.jced.7b01031.
[80] C. Guder, W. Wagner, A Reference Equation of State for the Thermodynamic Properties of Sulfur Hexafluoride (SF_6) for Temperatures from the Melting Line to 625 K and Pressures up to 150 MPa, J. Phys. Chem. Ref. Data. 38 (2009) 33–94.
[81] W. Wagner, A. Pruß, The IAPWS Formulation 1995 for the Thermodynamic Properties of Ordinary Water Substance for General and Scientific Use, J. Phys. Chem. Ref. Data. 31 (2002) 387–535. https://doi.org/10.1063/1.1461829.
[82] A. Jäger, E. Mickoleit, C. Breitkopf, Accurate and predictive mixture models applied to mixtures with CO2, Proceedings of the 3rd European Supercritical CO2 Conference. (2019). https://doi.org/10.17185/DUEPUBLICO/48891.
[83] A. Klamt, Conductor-like screening model for real solvents: a new approach to the quantitative calculation of solvation phenomena, J. Phys. Chem. 99 (1995) 2224–2235.
[84] A. Klamt, V. Jonas, T. Bürger, J.C. Lohrenz, Refinement and parametrization of COSMO-RS, J. Phys. Chem. A. 102 (1998) 5074–5085.
[85] A. Klamt, F. Eckert, COSMO-RS: a novel and efficient method for the a priori prediction of thermophysical data of liquids, Fluid Phase Equilib. 172 (2000) 43–72.
[86] A. Klamt, G. Schüürmann, COSMO: a new approach to dielectric screening in solvents with explicit expressions for the screening energy and its gradient, J. Chem. Soc., Perkin Trans. 2 (1993) 799–805. https://doi.org/10.1039/P29930000799.
[87] I.H. Bell, E. Mickoleit, C.-M. Hsieh, S.-T. Lin, J. Vrabec, C. Breitkopf, A. Jäger, A Benchmark Open-Source Implementation of COSMO-SAC, J. Chem. Theory Comput. 16 (2020) 2635–2646. https://doi.org/10.1021/acs.jctc.9b01016.
[88] R. Span, R. Beckmüller, T. Eckermann, S. Herrig, S. Hielscher, A. Jäger, E. Mickoleit, T. Neumann, S.M. Pohl, B. Semrau, M. Thol, TREND. Thermodynamic Reference and Engineering Data 4.0, Lehrstuhl fuer Thermodynamik, Ruhr-Universitaet Bochum, Bochum, Germany, 2019.
[89] E. Mullins, R. Oldland, Y.A. Liu, S. Wang, S.I. Sandler, C.-C. Chen, M. Zwolak, K.C. Seavey, Sigma-Profile Database for Using COSMO-Based Thermodynamic Methods, Ind. Eng. Chem. Res. 45 (2006) 4389–4415. https://doi.org/10.1021/ie060370h.
[90] J. Gernert, A. Jäger, R. Span, Calculation of Phase Equilibria for Multi-Component Mixtures Using Highly Accurate Helmholtz Energy Equations of State, Fluid Phase Equilib. 375 (2014) 209–218. https://doi.org/10.1016/j.fluid.2014.05.012.
[91] A. Jäger, Complex Phase Equilibria of Gas Hydrates and Other Solid and Fluid Phases Modeled with Highly Accurate Equations of State, Dissertation, Ruhr-Universität Bochum, 2016. https://hss-opus.ub.ruhr-uni-bochum.de/opus4/frontdoor/index/index/docId/4546 (accessed April 12, 2019).
[92] K. Brun, P. Friedman, R. Dennis, Fundamentals and applications of supercritical carbon dioxide (sCO2) based power cycles, 1st edition, Elsevier, Waltham, MA, 2017.
[93] EU, Regulation (EU) No 517/2014 of the European Parliament and of the Council of 16 April 2014 on fluorinated greenhouse gases and repealing Regulation (EC) No 842/2006, 2014. https://eur-lex.europa.eu/eli/reg/2014/517/oj/eng (accessed October 19, 2020).
[94] J.S. Daniel, G.J.M. Velders, A.R. Douglass, P.M.D. Forster, D.A. Hauglustaine, I.S.A. Isaksen, L.J.M. Kujipers, A. McCulloch, T.J. Wallington, Halocarbon Scenarios, Ozone Depletion Potentials, and Global Warming Potentials, Scientific Assessment of Ozone Depletion. (2016).
[95] I.H. Bell, A. Jäger, Calculation of Critical Points from Helmholtz-Energy-Explicit Mixture Models, Fluid Phase Equilib. 433 (2017) 159–173. https://doi.org/10.1016/j.fluid.2016.10.030.
[96] N. Polikhronidi, R. Batyrova, A. Aliev, I. Abdulagatov, Supercritical CO2: Properties and Technological Applications - A Review, J. Therm. Sci. 28 (2019) 394–430.
[97] N. Ribeiro, T. Casimiro, C. Duarte, M. Nunes da Ponte, A. Aguiar-Ricardo, M. Poliakoff, Vapor-Liquid Equilibrium and Critical Line of the CO_2 + Xe System. Critical Behavior

of CO_2 + Xe versus CO_2 + n-Alkanes, J. Phys. Chem. B. 104 (2000) 791–795.
[98] L. Calderazzi, P.C. di Paliano, Thermal stability of R-134a, R-141b, R-1311, R-7146, R-125 associated with stainless steel as a containing material, (1997) 9.
[99] F. Zeng, J. Tang, Q. Fan, J. Pan, X. Zhang, Q. Yao, J. He, Decomposition Characteristics of SF6 under Thermal Fault for Temperatures below 400 ℋ, 21 (2014) 10.
[100] R.J. Ferm, The Chemistry Of Carbonyl Sulfide, Chem. Rev. 57 (1957) 621–640. https://doi.org/10.1021/cr50016a002.

ANNEX A

EQUATIONS OF STATE USED FOR THE SCREENING

The multi-parameter equations of state used in the multi-fluid mixture model are listed in Table A1.

Table A1: Substances considered in the screening and references (Ref.) for multi-parameter equations of state used for these substances.

Substance (IUPAC name)	Ref.	Substance name used in this work
buta-1,3-diene	[31]	13butadiene
but-1-ene	[32]	1butene
but-1-yne	[31]	1butyne
pent-1-ene	[31]	1pentene
acetylene	[31]	acetylene
(2Z)-but-2-ene (cis-2-butene)	[32]	c2butene
ethene	[51]	ethylene
2-methylprop-1-ene (isobutene)	[32]	ibutene
propa-1,2-diene	[31]	propadiene
propene	[31]	propylene
propyne	[33]	propyne
(2E)-but-2-ene (trans-2-butene)	[32]	t2butene
2,2-dimethylbutane	[31]	22dimethylbutane
2,3-dimethylbutane	[31]	23dimethylbutane
n-butane	[36]	butane
ethane	[50]	ethane
n-hexane	[31]	hexane
2-methyl-butane (isopentane)	[34]	ipentane
2-methylpropane (isobutane)	[36]	isobutan
methane	[37]	methane
2,2-dimethylpropane (neopentane)	[34]	neopentn
n-pentane	[31]	pentane
propane	[56]	propane
benzene	[31,35]	benzene
cyclobutene	[31]	cyclobutene
cyclohexane	[39]	cyclohex
cyclopentane	[40]	cyclopen
cyclopropane	[33]	cyclopro
ethoxyethane	[63]	dee
methoxymethane (dimethyl ether)	[49]	dme
methanol	[41]	methanol
dry air (0.7812 N_2, 0.2096 O_2, 0.0092 Ar)	[42]	air[1]
argon	[43]	argon

Table A1 (continued)

Substance (IUPAC name)	Ref.	Substance name used in this work
carbon monoxide	[34]	co
deuterium	[44]	d2
fluorine	[54]	fluorine
helium	[31]	helium
krypton	[34]	krypton
neon	[31]	neon
nitrogen trifluoride	[55]	nf3
nitrogen	[45]	nitrogen
orthohydrogen	[46]	orthohyd
oxygen	[47]	oxygen
parahydrogen	[46]	parahyd
xenon	[34]	xenon
decafluorobutane	[31]	c4f10
dodecafluoropentane	[31]	c5f12
tetradecafluorohexane	[31]	c6f14
trifluoro(iodo)methane	[38]	cf3i
dodecafluoro-2-methylpentan-3-one	[48]	novec649
trichloro(fluoro)methane (R-11)	[57]	r11
1,1,2-trifluoroethene (R-1123)	[31]	r1123
1,1,2-trichloro-1,2,2-trifluoroethane (R-113)	[58]	r113
1,2-dichlorotetrafluoro-ethane (R-114)	[60]	r114
1-chloro-1,1,2,2,2-pentafluoroethane (R-115)	[38]	r115
hexafluoroethane	[34]	r116
dichloro(difluoro) methane (R-12)	[58]	r12
hexafluoropropene (R-1216)	[31]	r1216
(Z)-1-chloro-2,3,3,3-tetrafluoropropene (R-1224yd(Z))	[31]	r1224ydz
2,2-dichloro-1,1,1-trifluoroethane (R-123)	[65]	r123
trans-1-chloro-3,3,3-trifluoroprop-1-ene (R-1233zd(E))	[66]	r1233zde
2,3,3,3-Tetrafluoroprop-1-ene (R-1234yf)	[67]	r1234yf
(1*E*)-1,3,3,3-Tetrafluoro-1-propene (R-1234ze(E))	[68]	r1234zee

Table A1 (continued)

Substance (IUPAC name)	Ref.	Substance name used in this work
(Z)-1,3,3,3-tetrafluoro-prop-1-ene (R-1234ze(Z))	[31]	r1234zez
2-chloro-1,1,1,2-tetrafluoroethane (R-124)	[31]	r124
3,3,3-trifluoroprop-1-ene	[31]	r1243zf
1,1,1,2,2-Pentafluoro-ethane (R-125)	[69]	r125
chloro(trifluoro) methane (R-13)	[59]	r13
1,1,1,2-Tetrafluoroethane (R-134a)	[70]	r134a
tetrafluoromethane (R-14)	[60]	r14
1,1-difluoroethane (R-152a)	[71]	r152a
Fluoroethane (R-161)	[72]	r161
dichloro(fluoro) methane (R-21)	[60]	r21
Octafluoropropane (R-218)	[34]	r218
chloro(difluoro) methane (R-22)	[58]	r22
1,1,1,2,3,3,3-Heptafluoro-propane (R-227ea)	[38]	r227ea
trifluoromethane (R-23)	[61]	r23
1,1,1,2,3,3-hexafluoro-propane (R-236ea)	[73]	r236ea
1,1,1,3,3,3-hexafluoro-propane (R-236fa)	[74]	r236fa
1,1,2,2,3-pentafluoro-propane (R-245ca)	[75]	r245ca
1,1,1,3,3-pentafluoro-propane (R-245fa)	[76]	r245fa
difluoromethane (R-32)	[62]	r32
1,1,1,3,3-pentafluoro-butane (R-365mfc)	[38]	r365mfc
chloromethane (R-40)	[63]	r40
44 wt% R-125, 4 wt% R-134a, 52 wt% R143a (R-404a)	[77]	r404a[1]
23 wt% R-32, 25 wt% R-125, 52 wt% R-134a (R-407c)	[77]	r407c[1]
fluoromethane (R-41)	[34]	r41
50 wt% R-32, 50 wt% R-125 (R-410a)	[77]	r410a[1]
50 wt% R-125, 50 wt% R-143a (R-507a)	[77]	r507a[1]
octafluorocyclobutane (R-C-318)	[60]	rc318
(*Z*)-1,1,1,4,4,4-hexa-fluorobut-2-ene (R-1336mzz(Z))	[31]	re1336mzzz

Table A1 (continued)

Substance (IUPAC name)	Ref.	Substance name used in this work
1,1,1,2,2-pentafluoro-2-methoxyethane (R-245cb2)	[31]	re245cb2
1,1,1,3,3-pentafluoro-2-(1,1,1,3,3-pentafluoro-propan-2-yloxy)propane (R-245fa2)	[31]	re245fa2
1,1,1,2,2,3,3-heptafluoro-3-methoxypropane (R-347mcc)	[31]	re347mcc
chloroethene (vinyl chloride)	[31]	vinylchloride
propan-2-one (acetone)	[34]	acetone
ammonia	[31]	ammonia
chlorine	[25]	chlorine
carbonyl sulfide	[34]	cos
($^2H_2$)water (deuterium oxide)	[78]	d2o
oxyrane (ethylene oxide)	[52,53]	etyoxide
hydrogen sulfide	[34]	h2s
hydrogen chloride	[79]	hcl
nitrous oxide	[34]	n2o
2-methyloxirane	[31]	propyleneoxide
sulfur hexafluoride	[80]	sf6
sulfur dioxide	[64]	so2
water	[81]	water

[1] These mixtures have been treated as pseudo pure-fluids applying the noted pseudo pure-fluid equations of state.

DOI: 10.17185/duepublico/73965
URN: urn:nbn:de:hbz:464-20210330-111312-8